

# Soft Matter

Accepted Manuscript



This is an *Accepted Manuscript*, which has been through the Royal Society of Chemistry peer review process and has been accepted for publication.

*Accepted Manuscripts* are published online shortly after acceptance, before technical editing, formatting and proof reading. Using this free service, authors can make their results available to the community, in citable form, before we publish the edited article. We will replace this *Accepted Manuscript* with the edited and formatted *Advance Article* as soon as it is available.

You can find more information about *Accepted Manuscripts* in the [Information for Authors](#).

Please note that technical editing may introduce minor changes to the text and/or graphics, which may alter content. The journal's standard [Terms & Conditions](#) and the [Ethical guidelines](#) still apply. In no event shall the Royal Society of Chemistry be held responsible for any errors or omissions in this *Accepted Manuscript* or any consequences arising from the use of any information it contains.

**Nucleation and Propagation of Voltage-driven Wrinkles in an Inflated  
Dielectric Elastomer Balloon**

Guoyong Mao<sup>a</sup>, Xiaoqiang Huang<sup>a</sup>, Mazen Diab<sup>b</sup>, Tiefeng Li<sup>a</sup>, Shaoxing Qu<sup>\*a</sup>, Wei  
Yang<sup>a</sup>

<sup>a</sup> *Department of Engineering Mechanics, and Soft Matter Research Center  
(SMRC), Zhejiang University, Hangzhou 310027, China.*

<sup>b</sup> *School of Engineering, Brown University, Providence RI 02912, USA.*

**Abstract**

Dielectric elastomer (DE) transducers frequently undergo voltage-induced large deformation which may lead to mechanical instabilities. Here, we investigate wrinkle formation and propagation on the surface of a DE membrane mounted on an air chamber and subjected to a step voltage. Our experiments show that the geometric characteristics of the wrinkle morphology and the nucleation sites depend on the inflation pressure and the applied voltage. As the inflation pressure increases, the critical voltage to nucleate wrinkle decreases, while the location to nucleate the wrinkle shifts from the center to the boundary of the membrane. Moreover, by increasing the amplitude of the applied voltage, wrinkle morphology changes from stripe-like wrinkles to labyrinth-like wrinkles. Furthermore, we develop an analytical model to validate the experimental observations and map out the various wrinkle morphologies as a function of the applied pressure and voltage. This three dimensional phase diagram may guide the designs of new soft actuators.

**Keywords:** Dielectric elastomer, actuator, wrinkle

\* Corresponding author. E-mail: [squ@zju.edu.cn](mailto:squ@zju.edu.cn), Phone: +86-571-87952024

## 1. Introduction

Dielectric elastomer (DE), a typical soft active material, possesses various advantages including voltage-induced large deformation, high energy density, fast response, quiet operation, light weight and low cost. Due to its unique electromechanical property, DE, as a soft transducer, has a wide range of applications, such as artificial muscle, adaptive lens, particular film pattern, energy generator and so on.<sup>1-3</sup> A typical DE transducer consists of a DE membrane sandwiched between two compliant electrodes (such as carbon grease). When subjected to a high voltage, the membrane experiences out-of-plane contraction and large in-plane extension.

Previous studies showed that DE transducers, when actuated, may experience mechanical instabilities including pull-in instability, snap-through instability, wrinkling and creasing.<sup>4-7</sup> These instabilities may lead to the failure of DE transducers. Therefore, suppression of such instabilities is very crucial to robustly design and operate DE transducers. On the other hand, mechanical instabilities accompanied by large deformation can, if rationally harnessed, pave the way for new functions and applications.<sup>8</sup> Lu et al. utilized the bulging transition of a DE tube to amplify the electromechanical energy conversion.<sup>9</sup> Li et al. succeeded in obtaining a voltage-induced area-expansion of 1692% by harnessing the snap-through instability of DE membrane comprised of an elastomeric membrane mounted on an air chamber.<sup>5</sup>

Wang et al. devised a new method termed dynamic electrostatic lithography (DEL) to tune the size and shape of patterns on a large polymer surface.<sup>2</sup>

Several studies have reported on wrinkle instabilities of soft materials with varying modulus when subject to various stimuli, such as heating, solvent swelling, mechanical loading, capillarity and so on.<sup>10-17</sup> For such systems, critical strain and geometric characteristics of the wrinkles have been analyzed satisfactorily.<sup>12, 18-20</sup> Recently, Zhu et al. investigated wrinkling instability of a DE transducer. Their analysis revealed two types of transitions between the flat and the wrinkle states. In type I, flat state becomes unstable and wrinkle occurs simultaneously throughout the DE, while in type II, wrinkle nucleates in confined areas surrounded by coexistent flat areas.<sup>6, 21</sup> Following previous work, Kolloosche et al. discovered a new type of instability called wrinkle-to-wrinkle transition which demonstrates the important role playing by the viscoelasticity in the wrinkle formation of DE system.<sup>22</sup>

Most previous studies of wrinkling are limited to planar film/substrate system, and the system with curved substrate attracts few attentions.<sup>23</sup> Recently, Zhang et al. developed an approach to realize controlled wrinkling by inflating a stretched Au-PDMS bilayer structure.<sup>24</sup> Breid and Crosby succeeded in controlling the wrinkle pattern on curved substrate by using a swelling-based approach.<sup>25</sup> Here we adopt a system of a DE balloon with an air chamber, which can form series of wrinkle patterns by tuning the voltage and the inner pressure. Due to the fast response of DE, the distribution and the pattern of wrinkle can change rapidly.

In the present work, we conduct experimental and theoretical studies to

investigate wrinkling of a DE membrane subject to an inner pressure and a step voltage. In section 2, the experimental setup is illustrated. A theoretical model is presented in Section 3, to analyze wrinkling of the DE balloon. In section 4, the theoretical and experimental results are presented and discussed. Finally, a conclusion is given in section 5.

## 2. Experiment on voltage-induced wrinkling of a DE membrane

The DE balloon consists primarily of a circular membrane made of 3M VHB4905 with thickness  $H_0 = 1$  mm. The membrane is then mounted on an air chamber comprised of an opening acrylic barrel with radius  $R_C = 45$  mm, two times the radius of the unstretched membrane, and height  $H_C = 200$  mm (Fig. 1). Upon mounting, the membrane is sandwiched between two carbon crease electrodes. In both the experiment and the analysis, the prestretch is then fixed as  $\lambda_{\text{pre}} = 2$ , and therefore the radius of the membrane before applying the voltage is determined as  $r_0 = 45$  mm and the thickness as  $h = H_0 / \lambda_{\text{pre}}^2$ .

The air chamber is connected to an air pump and a manometer (AZ instrument corporation, pressure range: 0–33.45 kPa, resolution: 0.02 kPa, accuracy:  $\pm 0.3\%$  of full scale at  $\pm 25$  °C). The air is pumped into the chamber through a check valve until an inflation pressure is obtained after which the mass of the air is kept constant. The high power source, Trek 610E, is connected to a function generator (Agilent 33250A) to generate alternating voltage within the range of 0-10 kV. We use square wave alternating voltage to actuate the DE membrane. The frequency of the voltage is  $f$ , and

the amplitude of the voltage is recorded as  $\phi_A$ . The alternating voltage can be expressed as  $\phi = \frac{1}{2} \left(1 - \frac{|\sin \omega t|}{\sin \omega t}\right) \phi_A$ , ( $t > 0$ ), where  $\omega$  is the angular frequency.

In order to eliminate the Mullins effect, we first apply a low square wave alternating voltage,  $\phi = \frac{3}{2} \left(1 - \frac{|\sin 2\pi t|}{\sin 2\pi t}\right)$  kV, and an initial air pressure  $P_0 = 600$  Pa on the DE membrane for 10 minutes. Then the initial air pressure  $P_0$  will be varied between 200 Pa and 800 Pa by controlling the mass of the air. We take the square wave alternating voltage as a step voltage in one period. For each  $P_0$ , the amplitude of applied voltage varies as  $\phi_A = 4, 5, 6,$  and  $7$  kV. The frequency is kept constant as  $f = 1$  Hz. A high-speed camera with frame rate 1000/s is used to record the propagation of the wrinkles.

Our experiments revealed that once the amplitude of the applied voltage reaches a critical value, the wrinkle occurs. Interestingly, the nucleation location of the wrinkle moves along the longitudinal directions depending on the initial pressure,  $P_0$ . When  $P_0$  increases, the nucleation location moves from the top to the bottom of the inflated membrane as illustrated in Fig. 2. For example, when  $P_0$  is as small as 650 Pa, the wrinkle always nucleates from the top (Fig. 2(a)), and when  $P_0$  reaches 750 Pa, the wrinkle is observed to nucleate from the middle (Fig. 2(c)). However, when  $P_0$  is larger than 850 Pa, the wrinkle tends to nucleate from the bottom (Fig. 2(d)). Besides the nucleation location, the experiment demonstrates that the critical voltage to generate wrinkle also depends on the initial pressure  $P_0$ . Observation shows that the critical voltage increases as  $P_0$  decreases. For example, for an initial pressure,  $P_0 =$

600 Pa, wrinkle was observed for an applied voltage  $\phi_A = 5$  kV. When  $P_0 = 400$  Pa, the critical voltage for wrinkle is about 7 kV.

The wrinkle pattern is closely related to the voltage as shown in Fig. 3. As  $\phi_A (> \phi_c)$  increases, the wrinkling region expands and spreads from the top to the bottom of the membrane. Besides, the pattern of the wrinkle transits from regular stripes to irregular labyrinth. For the voltage near  $\phi_c$ , the wrinkle is mostly along the longitudinal direction as Fig. 3(a2) shows. As  $\phi_A$  increases, the direction of the wrinkle changes to be irregular near the top but remains regular on the edge of the wrinkling region (Fig. 3(b2)). If the voltage is large enough, the wrinkle pattern near the edge remains in the longitudinal direction, but the top of the DE membrane starts to collapse with a pattern resembling human cerebral cortex (Fig. 3(c2)).

Fig. 4 shows the snapshots indicating the evolution of wrinkle in one period of the step voltage with the initial pressure  $P_0 = 700$  Pa under  $\phi_A = 6$  kV (see movie S1) and  $\phi_A = 7$  kV (see movie S2). The maximum current of the power source is limited to  $I_{\max} = 2000 \mu\text{A}$ , and the capacity of the DE balloon is about  $C = 2.1$  nF. The charging time for the voltage of  $\phi = 6$  kV can be estimated as  $t = C\phi / I_{\max} = 6.3 \times 10^{-3}$  s

As shown in Fig. 4(a), the time for wrinkle nucleation is about 0.06 s, which is substantially larger than the charging time (also for Fig. 4(b)). So it is reasonable to assume that the Maxwell stress induced by the voltage is applied to the DE balloon instantly and the configuration of the DE balloon is almost the same before and after applying the voltage in a short time  $t < 0.06$  s. This assumption will be adopted in the

theoretical analysis.

### 3. Theoretical predictions of the wrinkle patterns

In this section, we propose an analytical model based on the field theory to investigate the wrinkling behavior of the inflated DE membrane. We take the following assumptions: (i) The shape change of the DE membrane during charging is assumed to be negligible; (ii) The total stress in the current configurations is the sum of the mechanical stress due to the air pressure and the Maxwell stress induced by the electric field; (iii) If either of the two in-plane stress components,  $s_1$  and  $s_2$  along the longitudinal and circumferential directions, becomes negative, the membrane wrinkles immediately.<sup>26</sup> Moreover, based on our experimental observations, we devise the following wrinkle criteria: If  $s_2 < 0$  and  $|s_1| < 0.5|s_2|$ , stripe wrinkles along the circumferential direction nucleate. If  $s_1 < 0$ ,  $s_2 < 0$  and  $|s_1| \geq 0.5|s_2|$ , labyrinth-like wrinkles emerge.

We use  $s_i^-$  ( $i=1, 2$ ) to denote the nominal stress components when the DE membrane is in its equilibrium state without the voltage and  $s_i^+$  as the nominal stress components after the voltage applied. According to the first two assumptions,

$$s_i^+ = s_i^- + s_i^M, \quad (1)$$

where  $s_i^M$  is the Maxwell stress.

Following the ideal DE field theory,<sup>5,27</sup> the Maxwell stress components caused by the electric field can be defined as

$$s_1^M = \varepsilon E^2 / \lambda_1, \quad (2)$$

$$s_2^M = \varepsilon E^2 / \lambda_2, \quad (3)$$

where  $\lambda_1$  and  $\lambda_2$  are the stretch ratios along the longitudinal and latitudinal directions.

$\varepsilon$  is the permittivity of the DE and the true electric field is  $E = \lambda_1 \lambda_2 \phi / H_0$ .

To account for the stiffening effect of the DE membrane,<sup>5</sup> the material is modeled using Gent model with the following free energy density,

$$W = -\frac{\mu}{2} J_{\text{lim}} \ln\left(1 - \frac{\lambda_1^2 + \lambda_2^2 + \lambda_3^2 - 3}{J_{\text{lim}}}\right), \quad (4)$$

where  $\mu$  is the shear modulus, and  $J_{\text{lim}}$  is a constant that represents the stretch limit of the elastomer. The nominal stress-stretch relation of DE without voltage are derived as

$$s_1^- = \frac{\mu(\lambda_1^2 - \lambda_3^2)}{\lambda_1(1 - (\lambda_1^2 + \lambda_2^2 + \lambda_3^2 - 3)/J_{\text{lim}})}, \quad (5)$$

$$s_2^- = \frac{\mu(\lambda_2^2 - \lambda_3^2)}{\lambda_2(1 - (\lambda_1^2 + \lambda_2^2 + \lambda_3^2 - 3)/J_{\text{lim}})}. \quad (6)$$

Deformation theory for thin membrane structures under mechanical loading are well developed in the literature. Here we follow the work by Adkins and Rivlin<sup>28</sup> to derive the governing equations. We assume that the DE membrane is axisymmetric along the  $z$  direction as shown schematically in Fig. 5. The deformation of the DE membrane is represented by two functions  $z(R)$  and  $r(R)$ , where  $z$  and  $r$  are the coordinates of a material point in the deformed state, and  $R$  is the coordinate of the same material point in the reference state. The stretch along the latitudinal direction is defined as  $\lambda_2 = r/R$ .

Fig. 5 demonstrates a material particle with radius from  $R$  to  $R+dR$  in the reference state, but with new radius from  $r(R)$  to  $r(R+dR)$  and height from  $z(R)$  to  $z(R+dR)$ . We define the slope angle of the particle relative to the latitudinal direction

as  $\theta(R)$ . The geometric relation yields the following two equations,

$$\frac{dr}{dR} = \lambda_1 \cos \theta, \quad (7)$$

$$\frac{dz}{dR} = -\lambda_1 \sin \theta. \quad (8)$$

Force balance along  $z$  direction (Fig. 5(c)) requires that

$$\frac{d}{dR} (HRs_1^- \sin \theta) = \lambda_1 \lambda_2 RP \cos \theta. \quad (9)$$

Also, force balance along the direction normal to  $z$  direction (Fig. 5(d)) is enforced by the following equation

$$\frac{d}{dR} (HRs_1^- \cos \theta) + \lambda_1 \lambda_2 RP \sin \theta = s_2^- H. \quad (10)$$

Eqs. (9) and (10) give the following two equations,

$$\frac{d\theta}{dR} = -\frac{s_2^- \sin \theta}{s_1^- R} + \frac{\lambda_1 \lambda_2 P}{s_1^- H}, \quad (11)$$

$$\frac{ds_1^-}{dR} = \frac{1}{R} (s_2^- \cos \theta - s_1^-). \quad (12)$$

Eqs. (7), (8), (11) and (12) are the governing equations that are solved for the four variables,  $r(R)$ ,  $z(R)$ ,  $\theta(R)$  and  $\lambda_1(R)$ , which require suitable boundary conditions.

We set the origin of the coordinates at the apex of the inflated DE membrane. Considering the axisymmetric deformation of the inflated membrane, the initial values at the apex of the DE balloon for the four governing equations are  $r(0) = 0$ ,  $z(0) = 0$ ,  $\theta(0) = 0$ ,  $\lambda_1(0) = \lambda_{\text{apx}}$  and they are used for the numerical integration of the governing equations. The value  $\lambda_{\text{apx}}$  is the prestretch at the apex of the DE balloon and is obtained by satisfying the boundary condition  $r(R_0) = R_C$ . Once the four governing equations are solved, the state of the DE membrane is determined.

In the following part, we adopt the following dimensionless parameters to

analyze the nucleation and propagation of wrinkle,

$$\bar{z} = \frac{z}{R_0}, \bar{R} = \frac{R}{R_0}, \bar{s}_1 = \frac{s_1}{\mu}, \bar{s}_2 = \frac{s_2}{\mu}, \bar{P}_0 = \frac{P_0}{\mu H_0 / R_0}, \bar{\phi} = \frac{\phi}{H_0 \sqrt{\mu / \varepsilon}}$$

Fig. 6 shows nominal stresses along the radial direction right before (solids lines) and after (dashed lines) the voltage is applied to the inflated DE membrane with initial prestretch,  $\lambda_{\text{pre}} = 2$ . After the voltage is applied, it is observed that the stress component  $\bar{s}_2$  becomes negative which causes wrinkling of the membrane according to assumption (iii) in section 3. Fig. 6 also demonstrates that wrinkle does not necessarily nucleate at the center of the DE membrane, but within a region that extends from  $\bar{R} \approx 0.2$  to  $\bar{R} \approx 0.6$ , which is consistent with the experimental observation in Fig. 2.

We now calculate the critical voltage  $\bar{\phi}_c$  at which  $\bar{s}_1$  and  $\bar{s}_2$  become negative as a function of the initial pressure  $\bar{P}_0$ . As shown in Fig. 7(a), if  $\bar{P}_0 < 1.148$ , the critical voltage is the same for  $\bar{s}_1$  and  $\bar{s}_2$ . But when  $\bar{P}_0 > 1.148$ , the critical voltage for  $\bar{s}_2$  is smaller than that for  $\bar{s}_1$ . We note here, that when  $\bar{s}_1 > 0$  and  $\bar{s}_2 < 0$ , the wrinkle pattern takes the form of stripes along the circumferential direction. This prediction is consistent with the experimental observation in Fig. 2(a). Fig. 7(b) & (7c) show the location where the nominal stress components  $\bar{s}_1$  and  $\bar{s}_2$  are zero at their corresponding critical voltages with different initial pressure  $\bar{P}_0$ . It is observed that when  $\bar{P}_0 \leq 1.148$ , wrinkle always nucleates at the center of the DE balloon. When  $\bar{P}_0 > 1.148$ , as the initial pressure increases, the critical voltage for  $\bar{s}_2$  is smaller than that for  $\bar{s}_1$ , which indicates that wrinkle will first appear along the circumferential direction as illustrated in Fig. 3. Additionally, when  $1.148 < \bar{P}_0 \leq 1.929$ , wrinkle

nucleates at the middle of the DE membrane and propagates towards the circular edge. When  $\bar{P}_0 > 1.929$ , wrinkle first nucleates from the circular edge of the DE membrane. Even when the voltage exceeds the critical value for  $\bar{s}_1$ , wrinkle along the circumferential direction will never occur in the region  $\bar{R} > 0.5$ .

Because the prestretch of DE membrane has considerable effect on the wrinkling behavior of the system, we conducted the experiments with  $\lambda_{\text{pre}} = 1$  and  $\lambda_{\text{pre}} = 3$  too. For the case with  $\lambda_{\text{pre}} = 1$ , there is no obvious wrinkle observed even when the voltage and the inner pressure increase, which indicates that the critical voltage is larger than 10 kV (maximum amplitude provided by the power source). The critical voltage for  $\lambda_{\text{pre}} = 3$  is smaller than that for  $\lambda_{\text{pre}} = 2$  under the same initial pressure.

#### 4. Wrinkling Phase Diagram for an inflated DE membrane

The analytical model is now used in combination with the experimental observations in section 2 to set wrinkling criteria for an inflated DE membrane subjected to voltage. The following criteria are extracted from the experimental observations and the analytical model in sections 2 and 3: (i)  $\bar{s}_1^+ > 0$  and  $\bar{s}_2^+ > 0$ , flat (no wrinkle); (ii)  $\bar{s}_1^+ > 0$  and  $\bar{s}_2^+ \leq 0$ , straight stripe wrinkle along longitudinal direction; (iii)  $|\bar{s}_1^+| < |0.5\bar{s}_2^+|$ ,  $\bar{s}_1^+ \leq 0$ , and  $\bar{s}_2^+ \leq 0$ , curved stripe wrinkle; (iv)  $|0.5\bar{s}_2^+| < |\bar{s}_1^+| \leq |0.9\bar{s}_2^+|$ ,  $\bar{s}_1^+ \leq 0$ , and  $\bar{s}_2^+ \leq 0$ , labyrinth wrinkle; (v)  $|0.9\bar{s}_2^+| < |\bar{s}_1^+| \leq |\bar{s}_2^+|$ ,  $\bar{s}_1^+ \leq 0$ , and  $\bar{s}_2^+ \leq 0$  irregular labyrinth wrinkle.

The above criteria are used to analyze the wrinkling behavior of the experimental observations in Fig. 3. Here, the shear modulus and permittivity of VHB 4905 are

taken as  $\mu = 50$  kPa and  $\varepsilon = 4.12 \times 10^{-11}$  F/m. The initial pressure is fixed as  $\bar{P}_0 = 1.17$  (650Pa). Fig. 8 shows the different wrinkling patterns that may emerge along the longitudinal direction as a function of the applied voltage. The Flat, straight stripe, curved stripe, labyrinth and irregular labyrinth patterns are indicated by blue, red, cyan, yellow and green colors on Fig. 8. The insets (a), (b) and (c) in Fig. 8 show that the analytical model predicts the experimental observations in Fig. 3(a2), (b2), and (c2) which correspond to the different applied voltages: (a)  $\bar{\phi} = 0.287$  (5 kV), (b)  $\bar{\phi} = 0.344$  (6 kV), and (c)  $\bar{\phi} = 0.402$  (7 kV).

Fig. 9 shows a three dimensional wrinkling phase diagram of the DE membrane. The diagram shows wrinkling behavior of the DE membrane under varying pressure and voltage. In particular, four inflation pressures representing the critical states in Fig. 7(b) & (c) are adopted. As shown in Fig. 9, the critical voltage for wrinkling is inversely proportional to the initial inflation pressure. Furthermore, for  $\bar{P}_0 = 0.8$  (within the range of  $\bar{P}_0 \leq 1.148$ ), wrinkle always nucleates from the center of the DE balloon, and labyrinth is the dominant pattern. We note here that the experiment does not show the labyrinth wrinkle pattern for low initial pressure. Instead a small circular region at the center of the DE balloon bulges out first and then wrinkles as shown in Fig. 2(a). We expect that under low inflation pressure, the DE membrane in the experiment may experience asymmetric deformation which cannot be captured by our axisymmetric model. When  $\bar{P}_0 = 1.2$  (within the range of  $1.148 < \bar{P}_0 \leq 1.41$ ), wrinkle always nucleates from the location away from the center of the DE balloon, and the wrinkle pattern takes the form of straight stripes along the circumferential direction

when the voltage is close to the critical value, as shown in Fig. 9(b). Fig. 9(c) shows the results for  $\bar{P}_0 = 1.6$  (within the range of  $1.41 < \bar{P}_0 \leq 1.929$ ), which are similar to those of  $\bar{P}_0 = 1.2$ . The difference is that the location where wrinkle nucleates moves further away from the center of the DE balloon, which can also be observed by comparing Fig. 9(b) and Fig. 9(c). When  $\bar{P}_0 = 2$  (within the range of  $\bar{P}_0 > 1.929$ ), wrinkle always nucleates from the bottom of the DE balloon Fig. 9(d).

## 5. Conclusion

We conducted both experiments and analytical modeling to investigate the wrinkling behavior of an initially inflated DE membrane subjected to a step voltage. Our experiments show that upon application of a step voltage the inflated DE membrane may wrinkle. In order to explain the experimental observations, an analytical model is developed and various wrinkling criteria are set.

Our experimental and analytical analyses show that the location and pattern of the wrinkle are dependent on the initial inflation pressure and the voltage applied. The nucleation and propagation of wrinkles within the DE membrane confirms the following observations:

(i) Both the critical voltage and the location for wrinkle nucleation are highly dependent on the inner pressure exerted on the DE balloon. As the inner pressure increases, the critical voltage will decrease, while the location where the wrinkle nucleates will shift from the center to the boundary of the DE balloon.

(ii) The amplitude of the voltage determines the pattern of wrinkle, i.e., the stripe

wrinkle occurs under a lower voltage, while the complex patterns such as labyrinth emerge under higher voltage.

Finally, the analytical predictions for wrinkling nucleation are consistent with the experimental data. However, the effects of prestretch and the volume of air chamber on the nucleation and propagation of wrinkles are not investigated and the analytical model fails to capture propagation of the wrinkle patterns beyond the critical voltage due to the dynamic nature of the wrinkle propagation. An analytical approach incorporating the inertia and viscous effects is desirable to predict the dynamic wrinkling accurately.

### **Acknowledgment**

This work is supported by the National Natural Science Foundation of China (Nos. 11222218, 11302190, 11321202, 11450110405), Zhejiang Provincial Natural Science Foundation of China (LQ13A020001, LZ14A020001), and the Fundamental Research Funds for the Central Universities.

## References

1. S. Shian, R. M. Diebold and D. R. Clarke, *Optics Express*, 2013, **21**, 8669-8676.
2. Q. Wang, M. Tahir, J. Zang and X. Zhao, *Advanced Materials*, 2012, **24**, 1947-1951.
3. R. Kaltseis, C. Keplinger, S. J. Adrian Koh, R. Baumgartner, Y. F. Goh, W. H. Ng, A. Kogler, A. Trols, C. C. Foo, Z. Suo and S. Bauer, *RSC Advances*, 2014, **4**, 27905-27913.
4. D. D. Tommasi, G. Puglisi, G. Saccomandi and G. Zurlo, *J. Phys. D, Appl. Phys.*, 2010, **43**, 325501.
5. T. Li, C. Keplinger, R. Baumgartner, S. Bauer, W. Yang and Z. Suo, *Journal of the Mechanics and Physics of Solids*, 2013, **61**, 611-628.
6. J. Zhu, M. Kolloosche, T. Lu, G. Kofod and Z. Suo, *Soft Matter*, 2012, **8**, 8840-8846.
7. Q. Wang and X. Zhao, *Physical Review E*, 2013, **88**, 042403.
8. X. Zhao and Q. Wang, *Applied Physics Reviews*, 2014, **1**, 021304.
9. T. Lu and Z. Suo, *Acta Mechanica Sinica*, 2012, **28**, 1106-1114.
10. N. Bowden, S. Brittain, A. G. Evans, J. W. Hutchinson and G. M. Whitesides, *Nature*, 1998, **393**, 146-149.
11. M. Guvendiren, S. Yang and J. A. Burdick, *Advanced Functional Materials*, 2009, **19**, 3038-3045.
12. E. Cerda and L. Mahadevan, *Physical Review Letters*, 2003, **90**, 074302.
13. H. Vandeparre, S. Gabriele, F. Brau, C. Gay, K. K. Parker and P. Damman, *Soft Matter*, 2010, **6**, 5751-5756.
14. J. M. Torres, C. M. Stafford and B. D. Vogt, *Soft Matter*, 2012, **8**, 5225-5232.
15. J. Huang, M. Juskiewicz, W. H. de Jeu, E. Cerda, T. Emrick, N. Menon and T. P. Russell, *Science*, 2007, **317**, 650-653.
16. M. Diab and K.-S. Kim, *Proceedings of the Royal Society of London A: Mathematical, Physical and Engineering Sciences*, 2014, **470**, 20140218.
17. A. Agrawal, P. Luchette, P. Palffy-Muhoray, S. L. Biswal, W. G. Chapman and R. Verduzco, *Soft Matter*, 2012, **8**, 7138-7142.
18. Z. Y. Huang, W. Hong and Z. Suo, *Journal of the Mechanics and Physics of Solids*, 2005, **53**, 2101-2118.
19. S. Cai, D. Breid, A. J. Crosby, Z. Suo and J. W. Hutchinson, *Journal of the Mechanics and Physics of Solids*, 2011, **59**, 1094-1114.
20. J. Genzer and J. Groenewold, *Soft Matter*, 2006, **2**, 310-323.
21. M. Kolloosche, J. Zhu, Z. Suo and G. Kofod, *Physical Review E*, 2012, **85**, 051801.
22. M. Kolloosche, G. Kofod, Z. Suo and J. Zhu, *Journal of the Mechanics and Physics of Solids*, 2015, **76**, 47-64.
23. X. Chen and J. Yin, *Soft Matter*, 2010, **6**, 5667-5680.
24. P. Zhang, D. Yang, Z. Li and H. Ma, *Soft Matter*, 2010, **6**, 4580-4584.
25. D. Breid and A. J. Crosby, *Soft Matter*, 2013, **9**, 3624-3630.
26. D. G. Roddeman, J. Drukker, C. W. J. Oomens and J. D. Janssen, *Journal of*

- Applied Mechanics*, 1987, **54**, 884-887.
27. Z. Suo, *Acta Mechanica Solida Sinica*, 2010, **23**, 549-578.
28. J. E. Adkins and R. S. Rivlin, *Philosophical Transactions of the Royal Society of London. Series A, Mathematical and Physical Sciences*, 1955, **248**, 201-223.

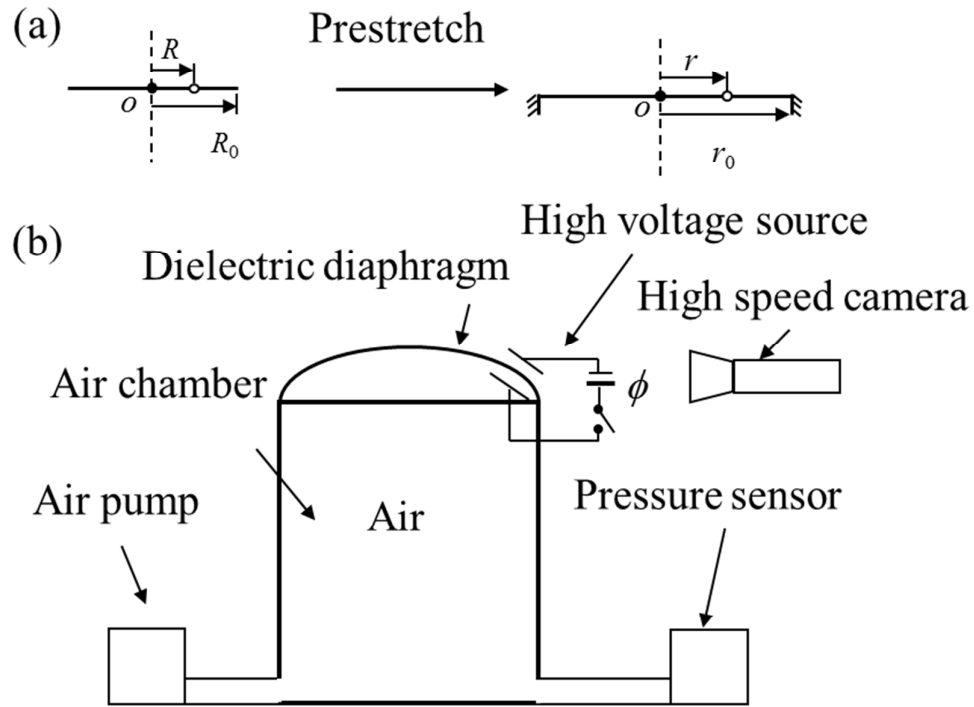


Figure 1. A schematic illustration of the experiment. (a) A sheet of circular membrane with radius  $R_0$  in the reference state and  $r_0$  in the deformed state after being prestretched. (b) Schematic diagram of the experimental set up. The prestretched membrane is mounted on an air chamber and actuated by air pressure and voltage.

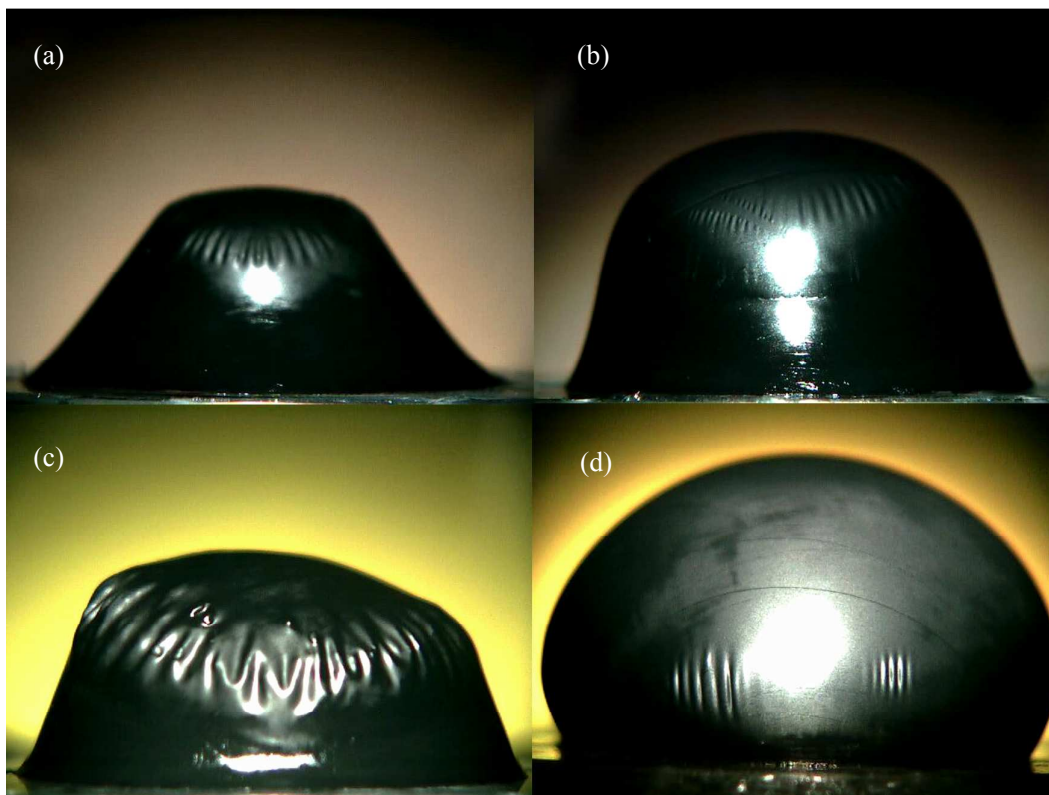


Figure 2. Evolution of the nucleation sites of wrinkles on the DE balloon as the initial pressure  $P_0$  increases. (a)  $P_0 = 650$  Pa,  $\phi_A = 5$  kV, (b)  $P_0 = 700$  Pa,  $\phi_A = 5$  kV, (c)  $P_0 = 750$  Pa,  $\phi_A = 5$  kV, and (d)  $P_0 = 850$  Pa,  $\phi_A = 5$  kV.

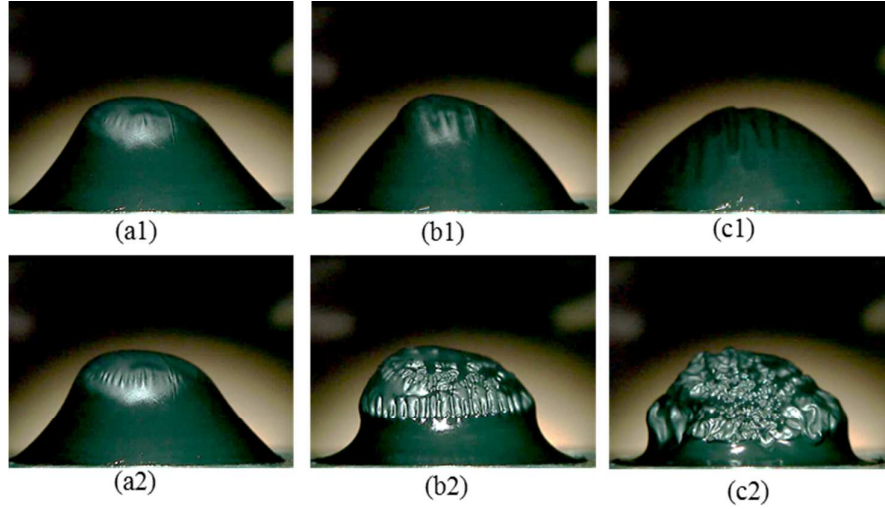


Figure 3: Evolution of the wrinkling pattern with initial pressure  $P_0 = 650$  Pa and increasing voltages of (a1, a2):  $\phi_A = 5$  kV, (b1, b2):  $\phi_A = 6$  kV, and (c1, c2):  $\phi_A = 7$  kV. The frequency of the voltage is fixed at  $f = 1$  Hz. The frames (a1), (b1) and (c1) are taken at 0.2 s and (a2), (b2) and (c2) at 0.5 s after applying the voltage.

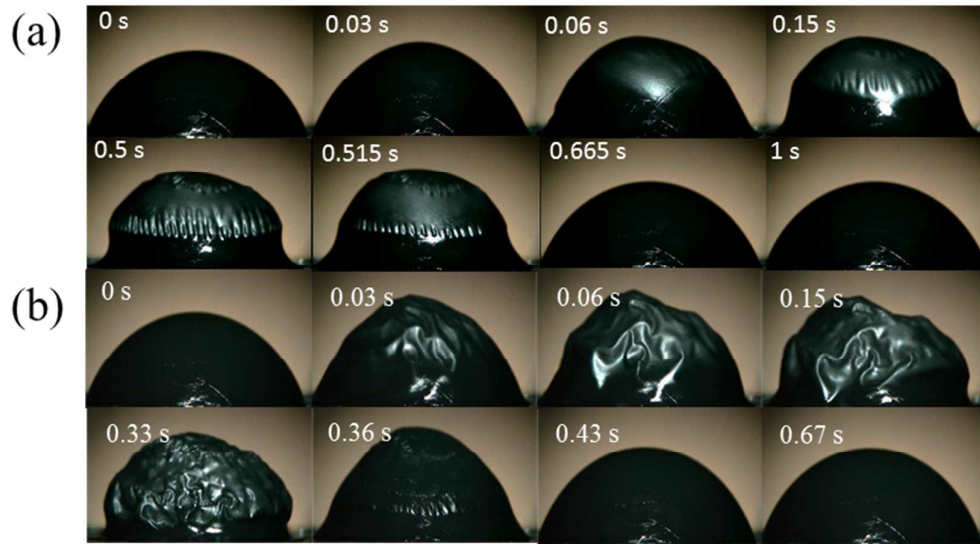


Figure 4. Evolution of wrinkle in one period of the step voltage,  $P_0 = 700$  Pa and (a)  $\phi_A = 6$  kV and (b)  $\phi_A = 7$  kV.

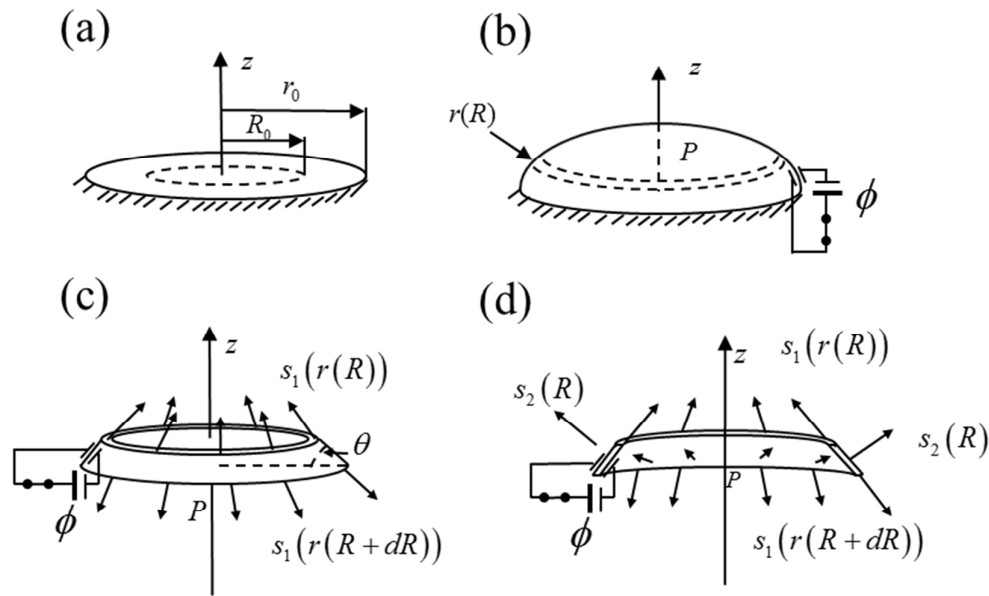


Figure 5. The free-body diagrams of a circular element in the DE balloon for (a) the deformed state after prestretch, (b) the deformed state after applying pressure and voltage, (c) force balance in the actuated state along  $z$  direction at  $r(R)$ , and (d) force balance for half of the truncated cone at  $r(R)$  along the direction perpendicular to  $z$  direction.

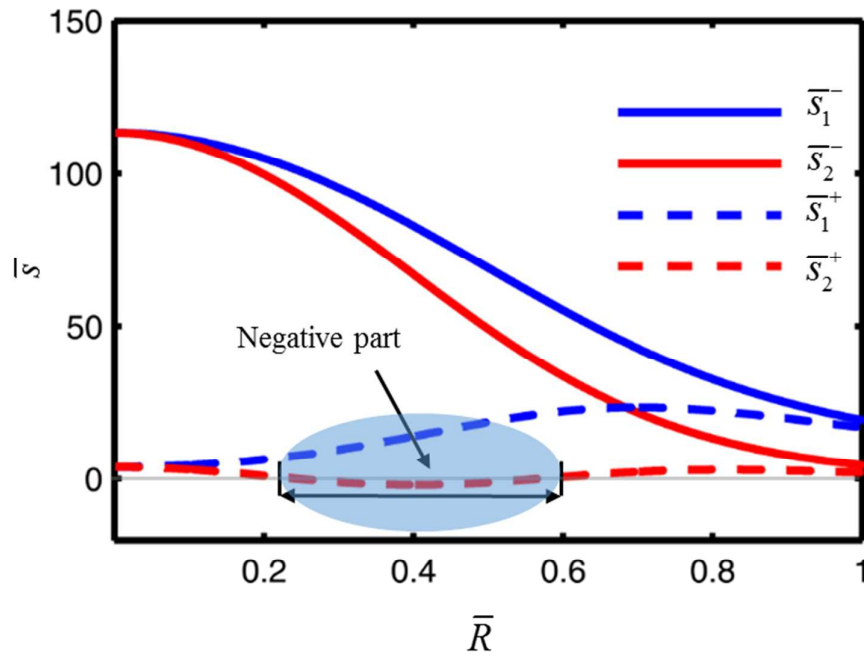


Figure 6. The stress states of the DE balloon in the reference coordinate system, before and after the voltage is applied with  $\lambda_{\text{pre}} = 2$ ,  $\bar{P}_0 = 1.2$  and  $\bar{\phi} = 0.185$ . The region where  $\bar{s}_2^+ < 0$  is encircled.

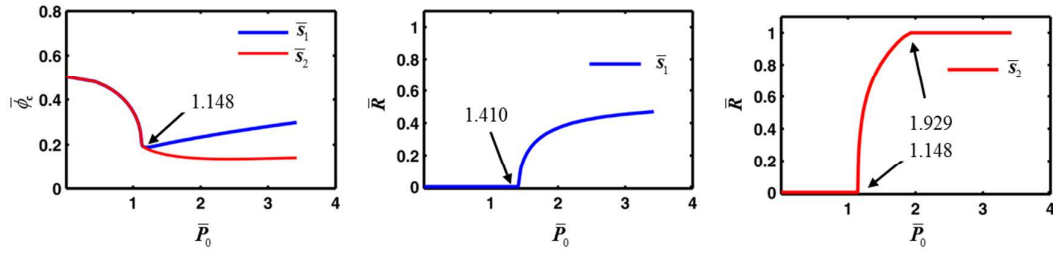


Figure 7. Theoretical predictions of the critical voltage and the location where wrinkles nucleate under different initial pressures. (a) Critical voltage vs. initial pressure for  $\bar{s}_1$  and  $\bar{s}_2$ . (b) Location where wrinkle nucleates vs. initial pressure  $\bar{s}_1$ . (c) Location where wrinkle nucleates vs. initial pressure  $\bar{s}_2$ . The prestretch is set as  $\lambda_{\text{pre}} = 2$ .

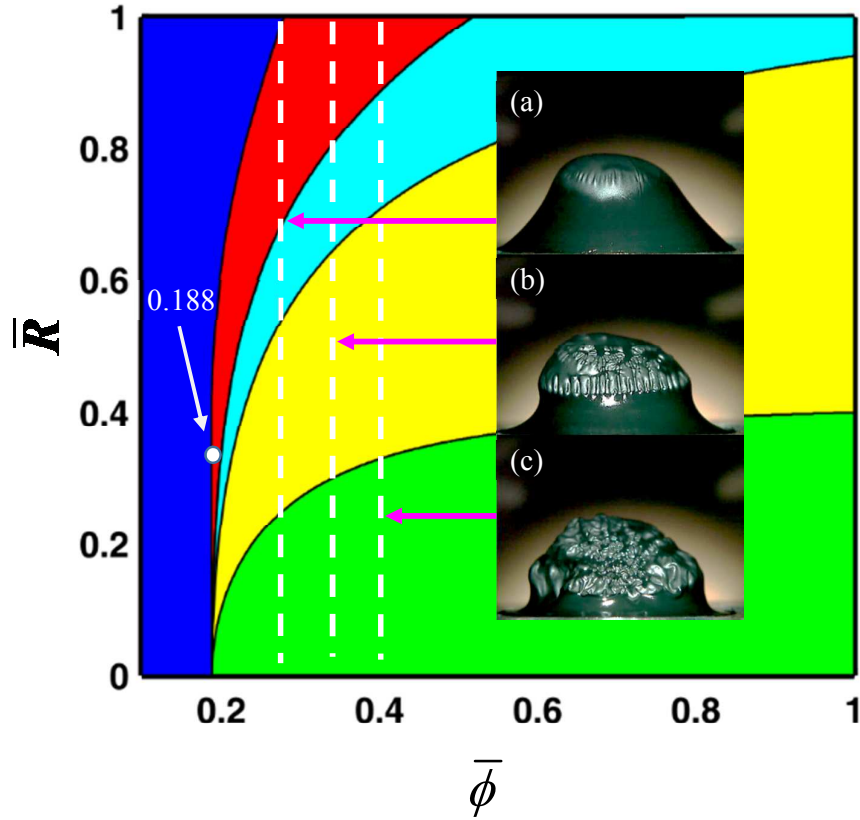


Figure 8. Distribution of the wrinkle patterns along the longitudinal direction with  $\bar{P}_0 = 1.17$  for various voltage  $\bar{\phi}$ . Three experimental wrinkle patterns for different voltages of (a)  $\bar{\phi} = 0.287$ , (b)  $\bar{\phi} = 0.344$ , and (c)  $\bar{\phi} = 0.402$  are shown. The critical voltage is  $\bar{\phi}_c = 0.188$  as marked in the figure. The stress states are indicated by (i) blue,  $\bar{s}_1^+ > 0$  and  $\bar{s}_2^+ > 0$ , (ii) red,  $\bar{s}_1^+ > 0$  and  $\bar{s}_2^+ \leq 0$ , (iii) cyan,  $|\bar{s}_1^+| < |0.5\bar{s}_2^+|$ ,  $\bar{s}_1^+ \leq 0$ , and  $\bar{s}_2^+ \leq 0$ , (iv) yellow,  $|0.5\bar{s}_2^+| < |\bar{s}_1^+| \leq |0.9\bar{s}_2^+|$ ,  $\bar{s}_1^+ \leq 0$ , and  $\bar{s}_2^+ \leq 0$ , and (v) green,  $|0.9\bar{s}_2^+| < |\bar{s}_1^+| \leq |\bar{s}_2^+|$ ,  $\bar{s}_1^+ \leq 0$ , and  $\bar{s}_2^+ \leq 0$ .

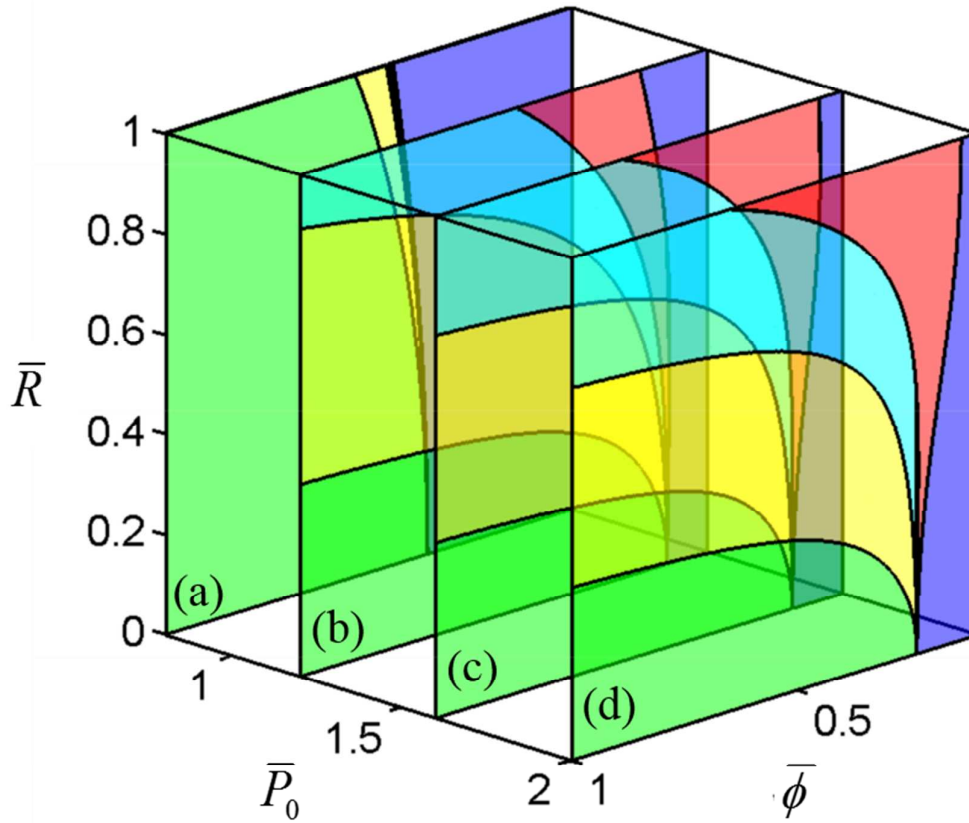


Figure 9. A 3D phase diagram showing distribution of the wrinkle patterns along the longitudinal direction as a function of the applied voltage for different initial pressures: (a)  $\bar{P}_0 = 0.8$ , (b)  $\bar{P}_0 = 1.2$ , (c)  $\bar{P}_0 = 1.6$ , and (d)  $\bar{P}_0 = 2$  with the same prestretch  $\lambda_{\text{pre}} = 2$ . Color codes are the same as those adopted by Fig. 8.